Chapter 2.

As-quenched Microstructures of

$Cu_{3-x}Mn_xAl$ Alloys

As-quenched Microstructures of $Cu_{3-x}Mn_xAl$ Alloys

Abstract

In the as-quenched condition, the microstructure of the $Cu_{2.9}Mn_{0.1}Al$ alloy was of $D0_3$ phase containing γ_1' martensite, where the $D0_3$ phase was formed by a $\beta \rightarrow B2 \rightarrow D0_3$ ordering transition during quenching. However, the as-quenched microstructure of the $Cu_{2.8}Mn_{0.2}Al$ or $Cu_{2.7}Mn_{0.3}Al$ alloy were found to be of $D0_3$ phase containing extremely fine L-J precipitates, whereas for $Cu_{2.6}Mn_{0.4}Al$ alloy, it was a mixture of ($D0_3$ + $L2_1$ + L-J) phases. These results are different from those proposed by Bouchard et al.

2-1 Introduction

By using thermal analysis method, Bouchard et al. have established the $Cu_{3-x}Mn_xAl$ ($0 \leqq X \leqq 1$) metastable phase diagram [1]. In that phase diagram, it is seen that when the $Cu_{3-x}Mn_xAl$ alloys with $0.1 \leqq X \leqq 0.8$ were solution-treated in the single β phase (disordered body-centered cubic(bcc)) region followed by a rapid quench into iced brine, a β → B2 → ($D0_3$ + $L2_1$) transition would occur by an ordering transition and a spinodal decomposition process, respectively. When the manganese (Mn) content in the $Cu_{3-x}Mn_xAl$ alloys was increased to 25 at.% (X=1), the as-quenched microstructure of the Cu_2MnAl alloy became a single $L2_1$ phase. In addition to the thermal analysis method, transmission electron microscopy (TEM) was also used by many workers to examine the as-quenched microstructures of the $Cu_{3-x}Mn_xAl$ alloys with $0.5 \leqq X \leqq 1.0$ [1-7]. These results were found to be consistent with those proposed by Bouchard et al.

Recently, we made TEM observations on the phase transformations of a $Cu_{2.2}Mn_{0.8}Al$ alloy [8]. Our experimental result indicated that the as-quenched microstructure of the $Cu_{2.2}Mn_{0.8}Al$ alloy consisted of a mixture of ($D0_3$ + $L2_1$ + L-J) phases, where the L-J phase is a new phase having an orthorhombic structure with lattice parameters a=0.413 nm, b=0.254 nm and c=0.728 nm [8]. This result is quite different from that reported by previous workers. However, to date, all of the TEM examinations were focused on the $Cu_{3-x}Mn_xAl$ alloys with $0.5 \leqq X \leqq 1$. Little information concerning the $Cu_{3-x}Mn_xAl$ alloys with lower Mn content has been provided. Therefore, the purpose of the present study is to

investigate the as-quenched microstructures of the $Cu_{3-x}Mn_xAl$ alloys with $X < 0.5$.

2-2 Experimental procedure

Four alloys, $Cu_{2.9}Mn_{0.1}Al$ (alloy A), $Cu_{2.8}Mn_{0.2}Al$ (alloy B), $Cu_{2.7}Mn_{0.3}Al$ (alloy C) and $Cu_{2.6}Mn_{0.4}Al$ (alloy D), were prepared in a vacuum induction furnace under a controlled protective Ar atmosphere by using 99.99% Cu, 99.9% Mn and 99.99% Al. The melts were chill cast into 30x50x200-mm-copper molds. After being homogenized at 900℃ for 72 hours, the ingots were sectioned into 2-mm-thick slices. These slices were subsequently solution heat-treated at 900℃ for 1 hour (in the single β-phase state) followed by a rapid quench into iced brine. The chemical compositions of the present alloys were analyzed by inductively coupled plasma-mass spectrometer (ICP), as shown in Table 2.1.

The microstructures of these alloys were examined by optical microscopy (OM) and transmission electron microscopy (TEM). TEM specimens were prepared by means of a double-jet electropolisher with an electrolyte of 70% methanol and 30% nitric acid. The polishing temperature was kept in the range from -30℃ to -15℃, and the current density was kept in the range from $3.0x10^4$ to $4.0x10^4$ A/m^2. Electron microscopy was performed on a JEOL JEM-2000FX scanning transmission electron microscope operating at 200 KV.

Table 2.1 Atomic and Chemical compositions of the present alloys by inductively coupled plasma-mass spectrometer (ICP)

Alloy number	Atomic composition ($Cu_{3-x}Mn_xAl$)	Designed compositions (at.%)			
		Cu	Al	Mn	X
A	$Cu_{2.9}Mn_{0.1}Al$	Bal.	25.1	2.7	0.108
B	$Cu_{2.8}Mn_{0.2}Al$	Bal.	25.3	5.1	0.202
C	$Cu_{2.7}Mn_{0.3}Al$	Bal.	25.1	7.6	0.303
D	$Cu_{2.6}Mn_{0.4}Al$	Bal.	25.2	10.3	0.409

2-3 Results and discussion

A. Optical microscopy observations:

The microstructures of the present alloys with equivalent Al content about 25 at.% where Mn varies from 2.7 to 10.3 at.% were shown in Figure 2.1. All of them were solution-treated at 900℃ for 1 hour (in the single β phase state) followed by a rapid quench into iced brine. Figure 2.1(a) shows the as-quenched microstructure of $Cu_{2.9}Mn_{0.1}Al$ alloy consisting of plate-like martensite; others were a single β phase. Based on the above results, it is concluded that the martensite transformation temperature would be decreased below to room temperature with increasing the Mn content up to 5.1 at.%. This result is in agreement with that reported by other workers in the Cu-Mn-Al alloy systems [9-11].

B. Transmission electron microscopy observations:

Figure 2.2(a) is a bright-field (BF) electron micrograph of the as-quenched $Cu_{2.9}Mn_{0.1}Al$ alloy, clearly exhibiting a second phase with a plate-like morphology within the matrix. Figures 2.2(b) through (d) show three selected-area diffraction patterns (SADPs) taken from a plate-like phase and its surrounding matrix. In these SADPs, it is seen that beside those reflection spots corresponding to the $D0_3$ phase [12-15], extra spots caused by the second phase are clearly visible. Compared with the previous studies in Cu-Al and Cu-Al-Ni alloys [15-17], it can be realized that the positions and streaking behaviors of the extra spots are the same as those of the γ_1' martensite

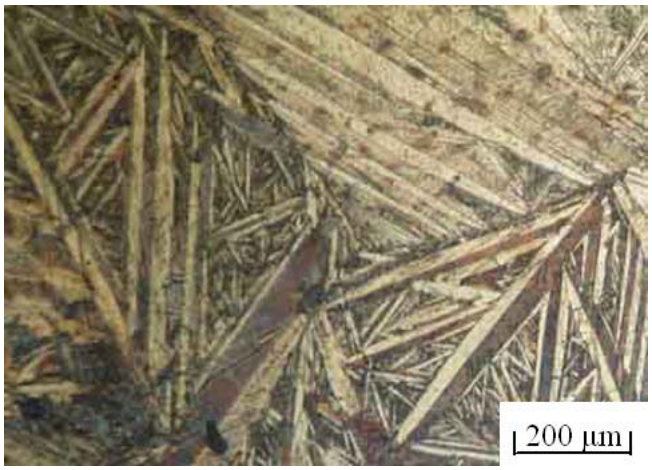

Figure 2.1(a)

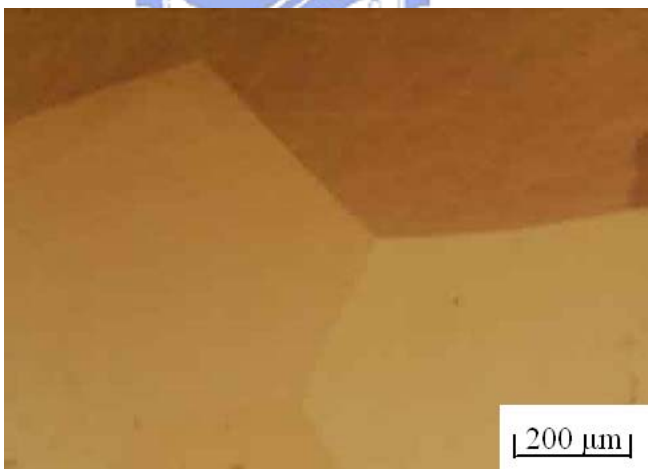

Figure 2.1(b)

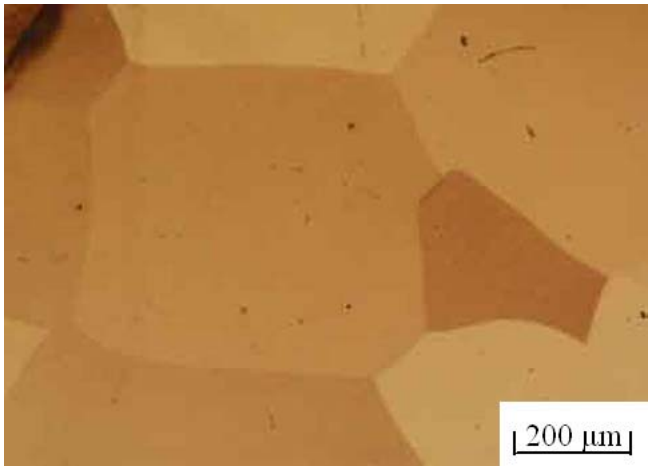

Figure 2.1(c)

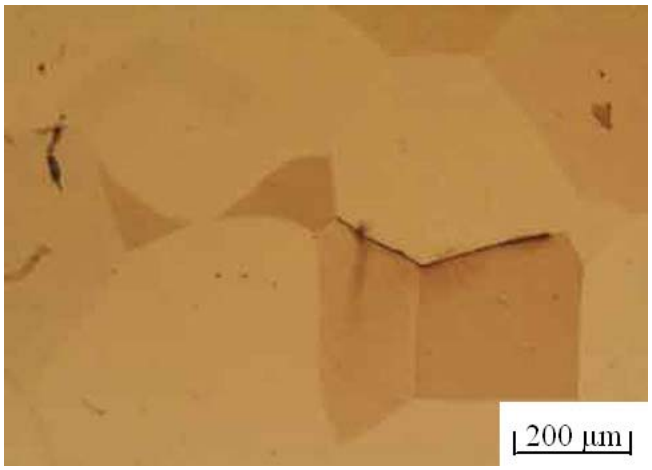

Figure 2.1(d)

Figure 2.1 Influence of Manganese concentration on the microstructures of Cu-Mn-Al alloys. (a) $Cu_{2.9}Mn_{0.1}Al$. (b) $Cu_{2.8}Mn_{0.2}Al$. (c) $Cu_{2.7}Mn_{0.3}Al$. (d) $Cu_{2.6}Mn_{0.4}Al$.

with internal twins. The γ_1' martensite has an orthorhombic structure with lattice parameters a=0.440 nm, b=0.534 nm and c=0.422 nm [15, 18]. Figure 2.2(e) is a $(1\bar{1}1)$ $D0_3$ dark-field (DF) electron micrograph of the same area as Figure 2.3(a), revealing the presence of the fine $D0_3$ domains with a/2<100> anti-phase boundaries (APBs). Figure 2.2(f), a (200) $D0_3$ DF electron micrograph, shows the presence of the small B2 domains with a/4<111> APBs. In Figures 2.2(e) and (f), it is seen that the sizes of both $D0_3$ and B2 domains are very small. Therefore, it is deduced that the $D0_3$ phase present in the as-quenched alloy was formed by a β → B2 → $D0_3$ continuous ordering transition during quenching [19-21]. Figure 2.2(g) is a $(1\bar{2}1)$ γ_1' DF electron micrograph, clearly revealing the presence of the plate-like γ_1' martensite. Accordingly, it is concluded that the as-quenched microstructure of the $Cu_{2.9}Mn_{0.1}Al$ alloy was $D0_3$ phase containing plate-like γ_1' martensite, where the $D0_3$ phase was formed by a β → B2 → $D0_3$ continuous ordering transition during quenching. This finding is different from that reported by other workers in the Cu_3Al alloy [1, 16].

When the Mn content was increased to 5.1 at.%, no evidence of the γ_1' martensite could be detected, rather a high density of extremely fine precipitates with a mottled structure could be observed within the $D0_3$ matrix. A typical example is shown in Figure 2.3. Figure 2.3(a) is a BF electron micrograph of the $Cu_{2.8}Mn_{0.2}Al$ alloy in the as-quenched condition. Figures 2.3(b) through (d) show three SADPs of the as-quenched alloy. When compared with our previous studies in the $Cu_{2.2}Mn_{0.8}Al$ and Cu-14.2Al-7.8Ni alloys [8, 15], it is found, in these SADPs, that the extra spots with streaks

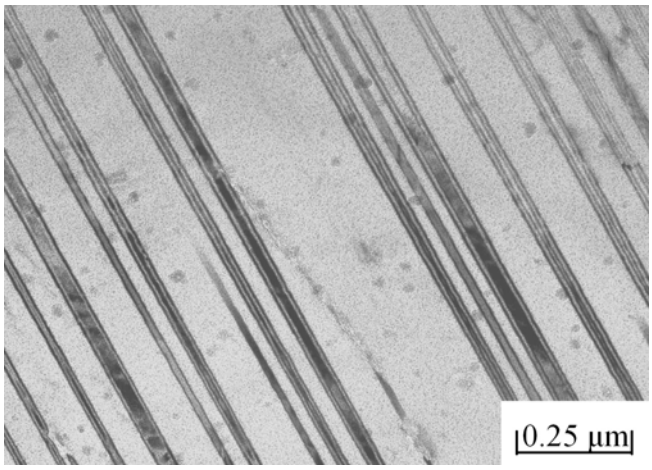

Figure 2.2(a)

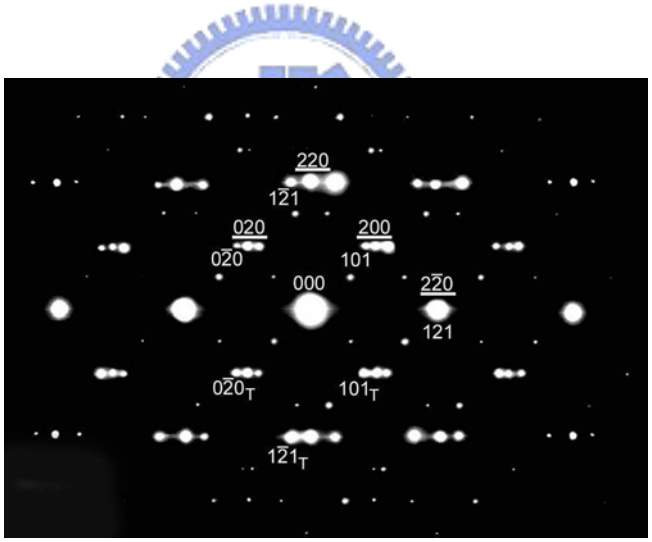

Figure 2.2(b)

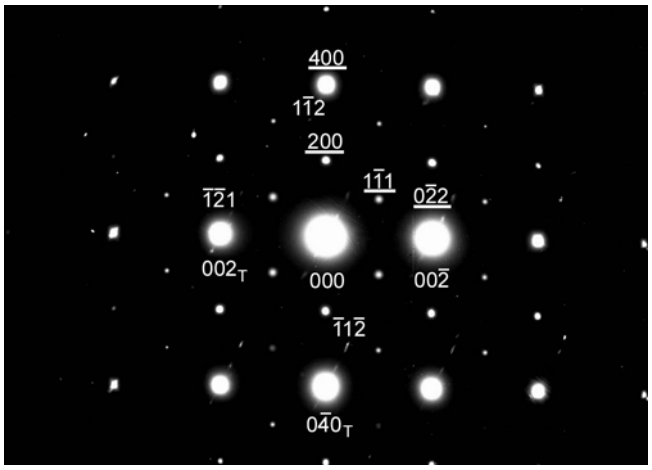

Figure 2.2(c)

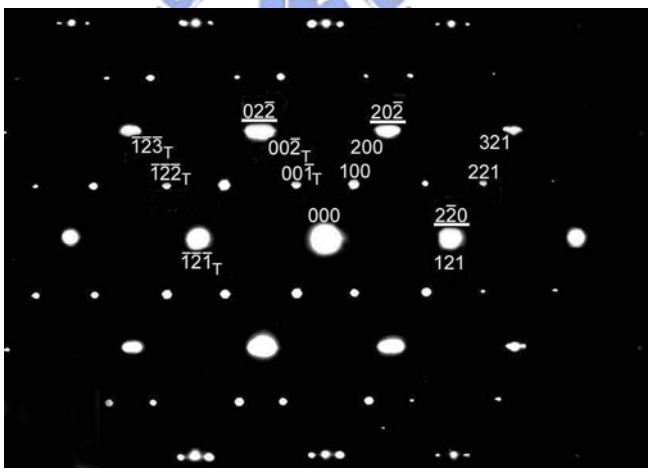

Figure 2.2(d)

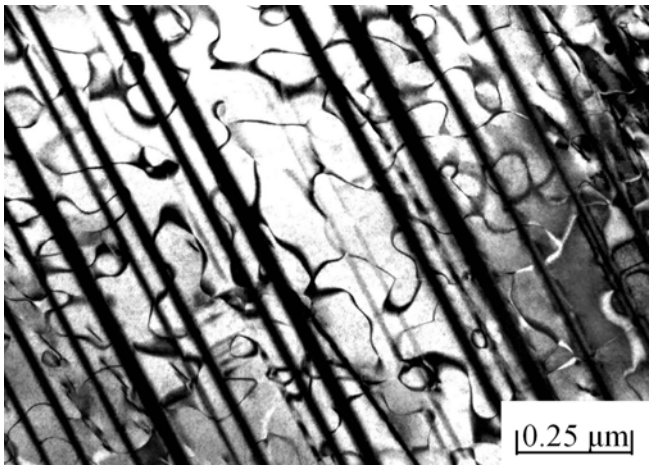

Figure 2.2(e)

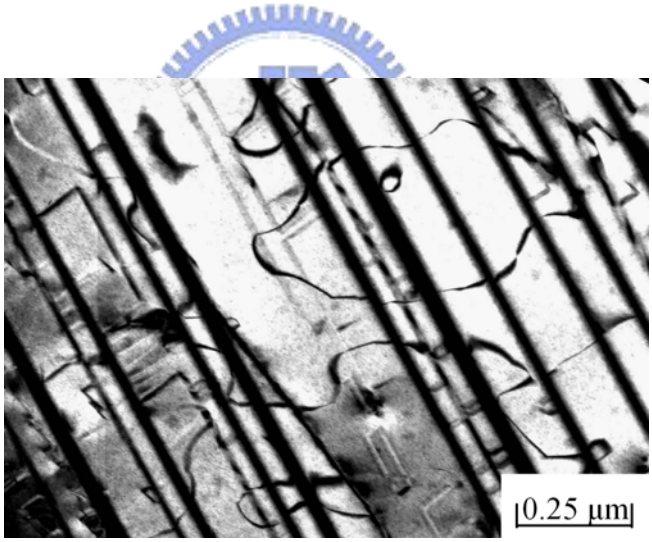

Figure 2.2(f)

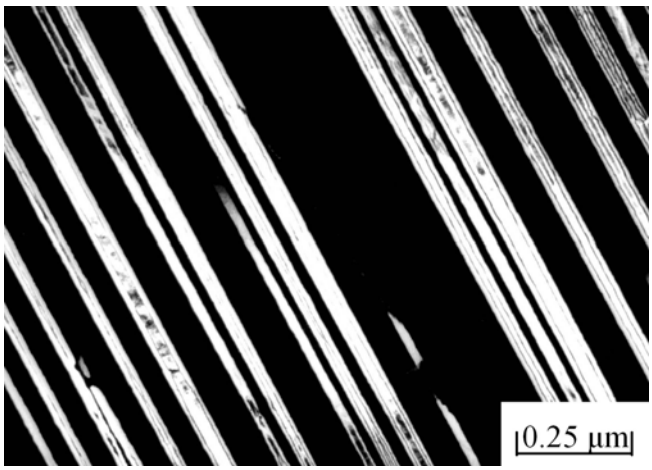

Figure 2.2(g)

Figure 2.2 Electron micrographs of the as-quenched $Cu_{2.9}Mn_{0.1}Al$ alloy. (a) BF, (b) through (c) three SADPs. The zone axes of the $D0_3$ phase, γ_1' martensite and internal twin are (b) $[001]$, $[10\bar{1}]$ and $[\bar{1}01]$, (c) $[011]$, $[1\bar{1}\bar{1}]$ and $[\bar{1}00]$ (d) $[111]$, $[01\bar{2}]$ and $[\bar{2}10]$, respectively (<u>hkl</u>= $D0_3$ phase, hkl=γ_1' martensite, hkl_T=internal twin). (e) and (f) $(1\bar{1}1)$ and (200) $D0_3$ DF, respectively, (g) $(1\bar{2}1)$ γ_1' DF.

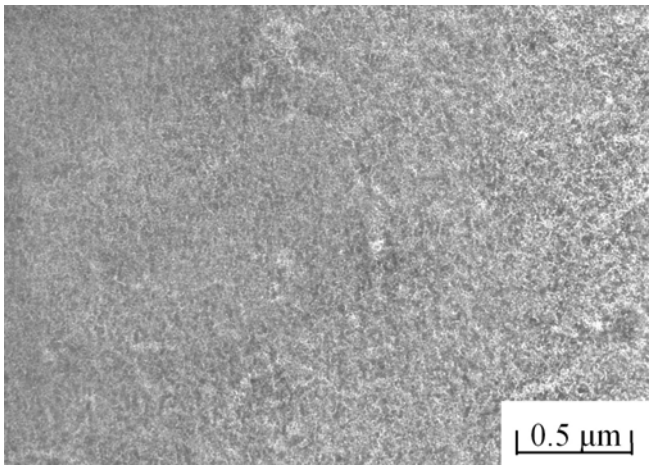

Figure 2.3(a)

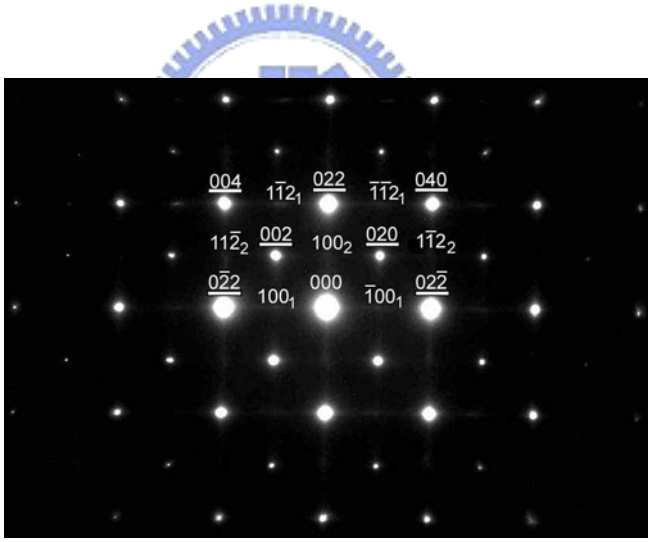

Figure 2.3(b)

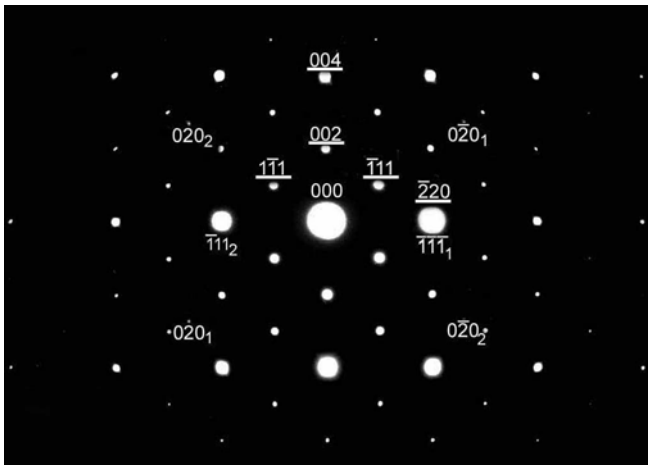

Figure 2.3(c)

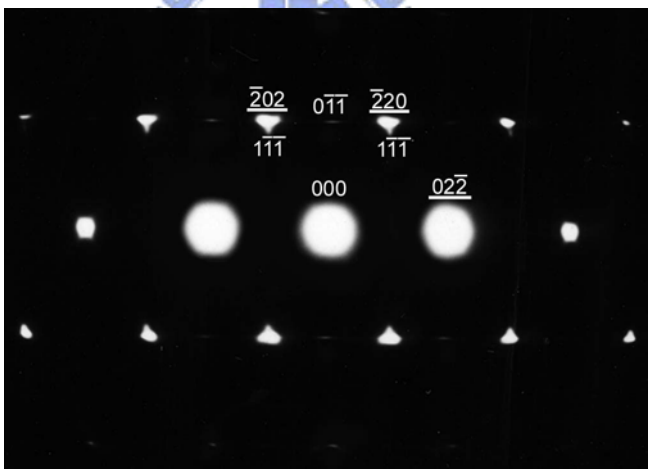

Figure 2.3(d)

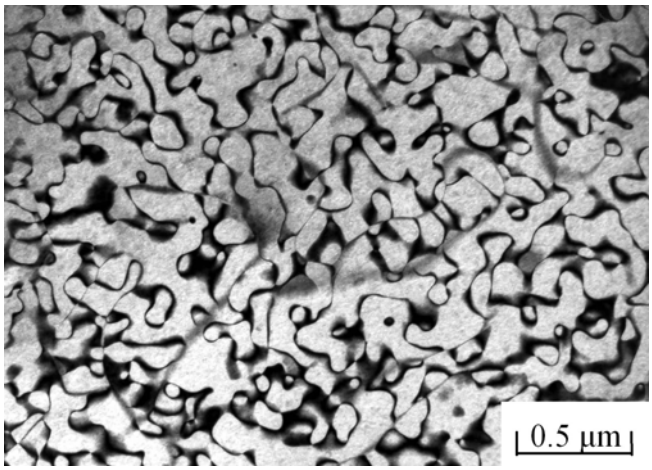

Figure 2.3(e)

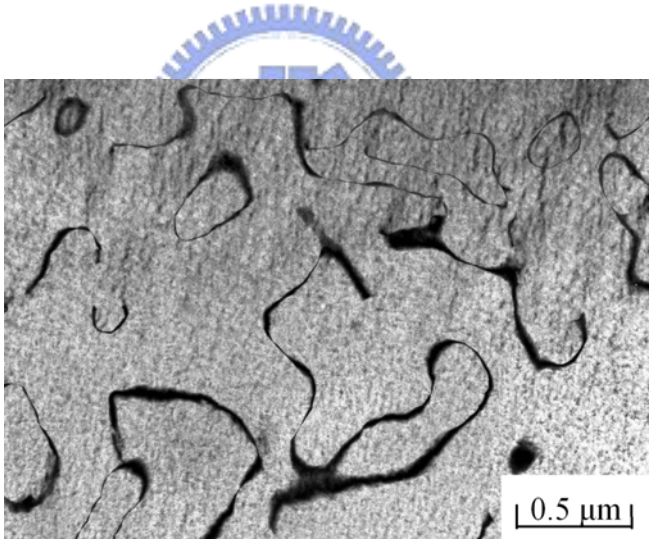

Figure 2.3(f)

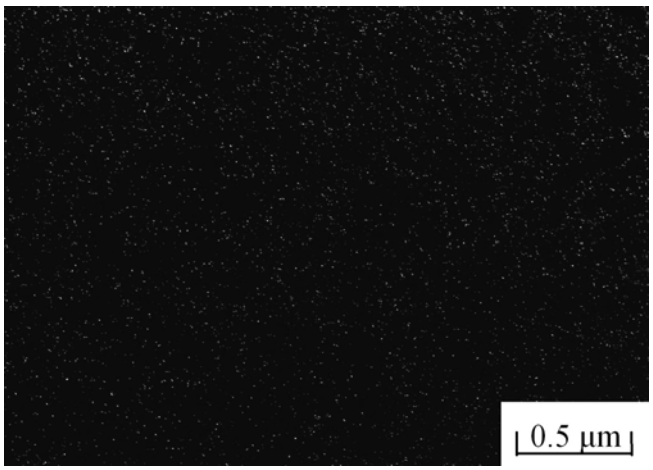

Figure 2.3(g)

Figure 2.3 Electron micrographs of the as-quenched $Cu_{2.8}Mn_{0.2}Al$ alloy. (a) BF, (b) through (d) three SADPs. The zone axes of the $D0_3$ phase are $[100]$, $[110]$ and $[111]$, respectively (<u>hkl</u>= $D0_3$ phase, hkl_{1or2}= L-J phase, 1: variant 1; 2: variant 2). (e) and (f) $(\bar{1}11)$ and (002) $D0_3$ DF, respectively, (g) (100_1)L-J DF.

could be derived from the L-J phase with two variants. Figure 2.3(e) and (f) are $(\bar{1}11)$ and (002) $D0_3$ DF electron micrographs of the same area as Figure 2.3(a), revealing the presence of the fine $D0_3$ domains with a/2<100 > APBs and the small B2 domains with a/4<111 > APBs, respectively. Figure 2.3(g) is a (100_1) L-J DF electron micrograph, exhibiting the presence of the extremely fine L-J precipitates. Based on the above observations, it was concluded that the as-quenched microstructure of the $Cu_{2.8}Mn_{0.2}Al$ alloy was $D0_3$ phase containing extremely fine L-J precipitates, where the $D0_3$ phase was formed by the β → B2 → $D0_3$ continuous ordering transition during quenching.

Transmission electron microscopy examinations of thin foils indicated that the as-quenched microstructure of the $Cu_{2.7}Mn_{0.3}Al$ alloy was also $D0_3$ phase containing extremely fine L-J precipitates, which is similar to that observed in the $Cu_{2.8}Mn_{0.2}Al$ alloy. An example is shown in Figure 2.4. By comparing Figures 2.3 and 2.4, it is clear that a slight increase of the Mn content would significantly raise the amount of the L-J precipitates; it would also increase the sizes of both B2 and $D0_3$ domains. Figure 2.5(a) is a BF electron micrograph of the as-quenched $Cu_{2.6}Mn_{0.4}Al$ alloy, exhibiting a modulated structure. Figures 2.5(b) and (c) are two SADP of the as-quenched alloy. In Figure 2.5(b), it is seen that in addition to the reflection spots with streaks of the L-J phase, the superlattice reflection spots with satellites lying along <001> reciprocal lattice directions could be clearly observed. Compared with the previous studies in the $Cu_{3-x}Mn_xAl$ alloys with x=0.5 or x=0.8 [1, 8], it is obvious that these supperlattice reflection spots with satellites were attributed to the coexistence of the ($D0_3$ + $L2_1$) phases. The ($D0_3$ Figure 2.5(c), a $(\bar{1}11)$ $D0_3$ DF electron micrograph,

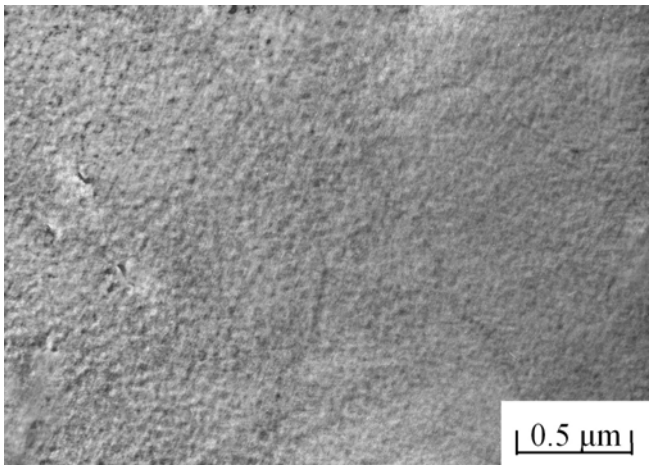

Figure 2.4(a)

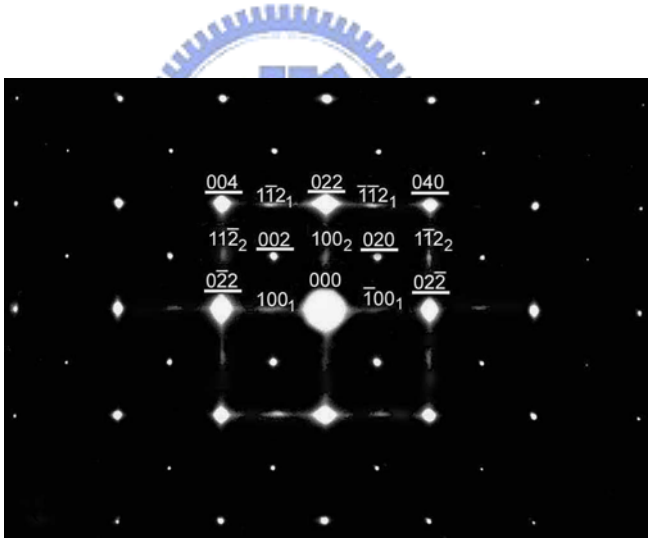

Figure 2.4(b)

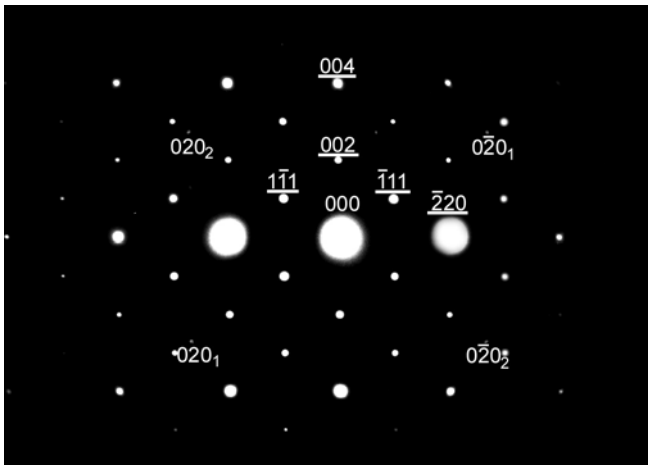

Figure 2.4(c)

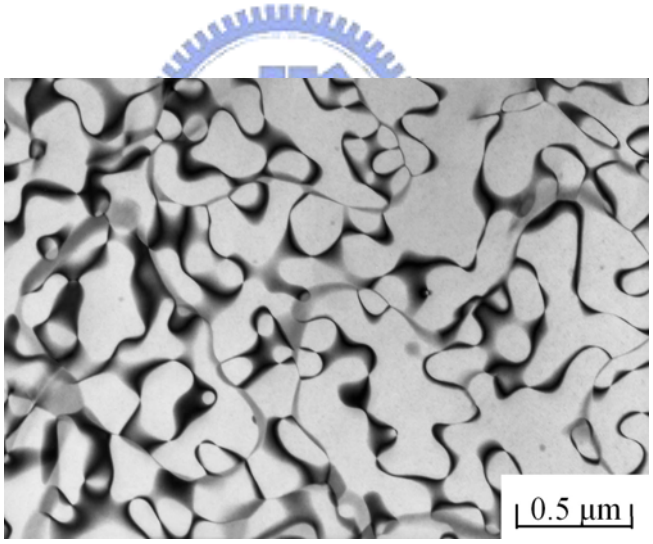

Figure 2.4(d)

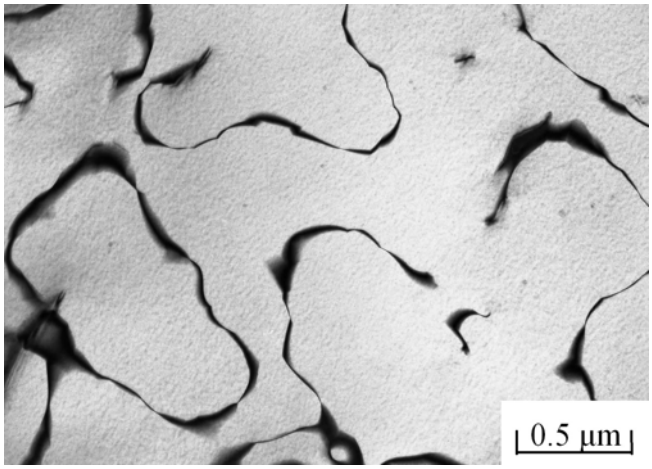

Figure 2.4(e)

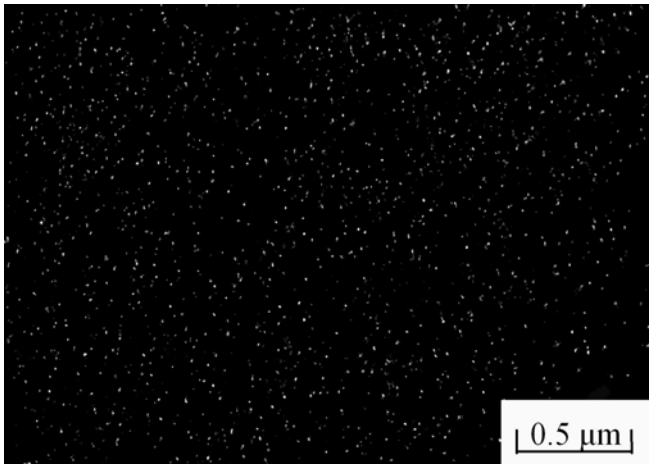

Figure 2.4(f)

Figure 2.4 Electron micrographs of the as-quenched $Cu_{2.7}Mn_{0.3}Al$ alloy. (a) BF, (b) and (c) two SADPs. The zone axes of the $D0_3$ phase are $[100]$ and $[110]$, respectively. (<u>hkl</u>= $D0_3$ phase, hkl_{1or2}= L-J phase, 1: variant 1; 2: variant 2). (d) and (e) $(\bar{1}11)$ and (002) $D0_3$ DF, respectively. (f) (100_1) L-J DF.

reveals the presence of the $D0_3$ domains with a/2<100> APBs. Figures 2.5(d) is a (002) $D0_3$ DF electron micrograph; no evidence of the a/4<111> APBs could be detected. This feature is similar to that observed in the as-quenched $Cu_{3-x}Mn_xAl$ alloys with $0.5 \leqq X \leqq 1.0$ [1-2, 8]. Figure 2.5(e), a DF electron micrograph taken with the (100_1) L-J reflection spot, exhibits that the amount of the extremely fine L-J precipitates was greater than that observed in Figures 2.3 and 2.4. As a consequence, the as-quenched microstructure of the $Cu_{2.6}Mn_{0.4}Al$ alloy was the mixture of ($D0_3$ + $L2_1$ + L-J) phases.

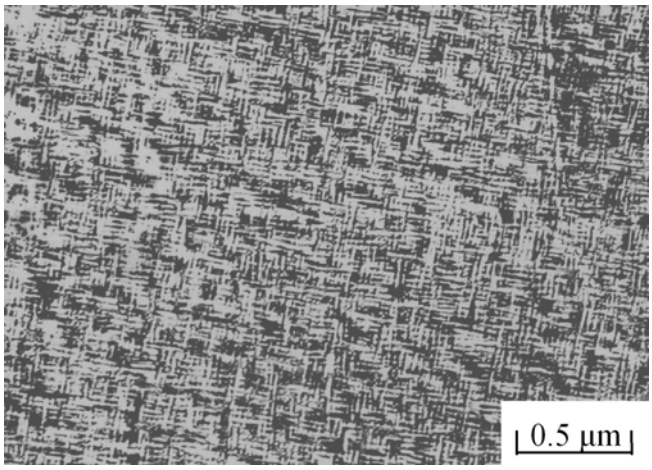

Figure 2.5(a)

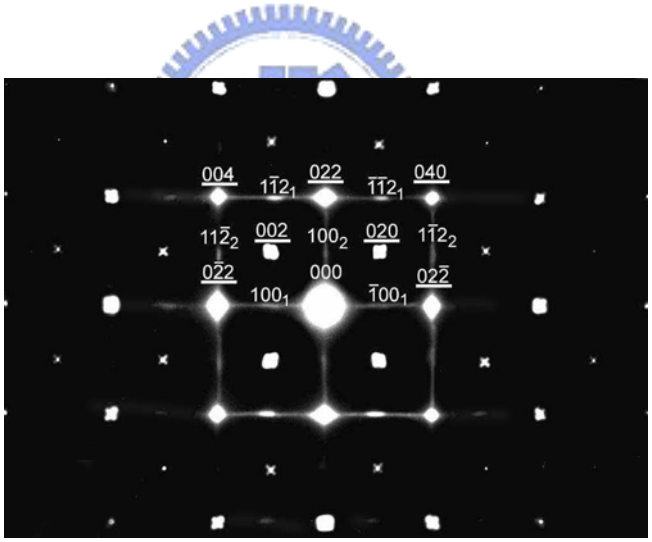

Figure 2.5(b)

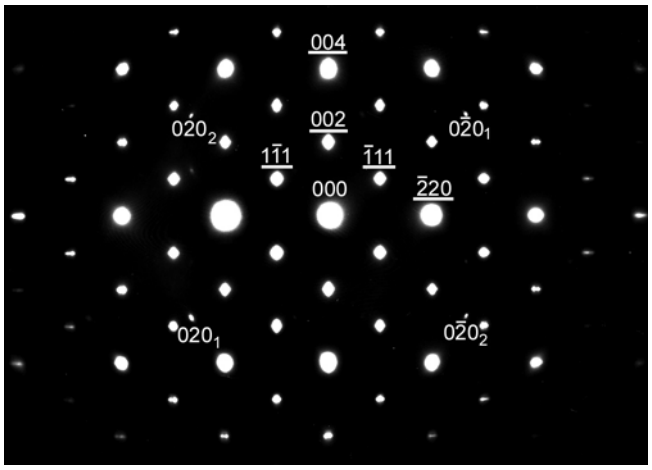

Figure 2.5(c)

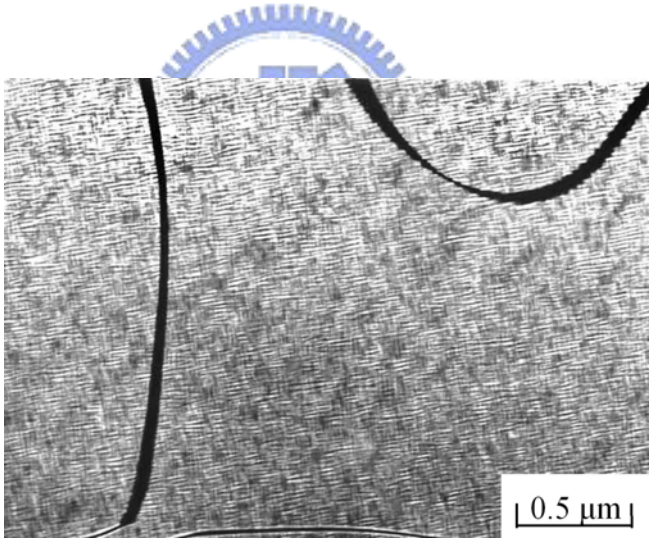

Figure 2.5(d)

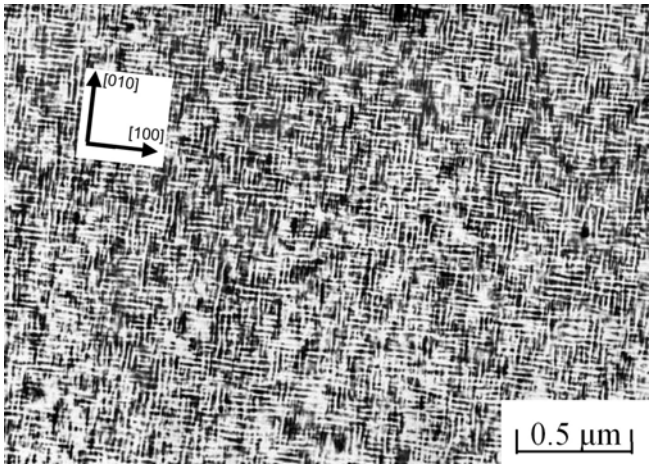

Figure 2.5(e)

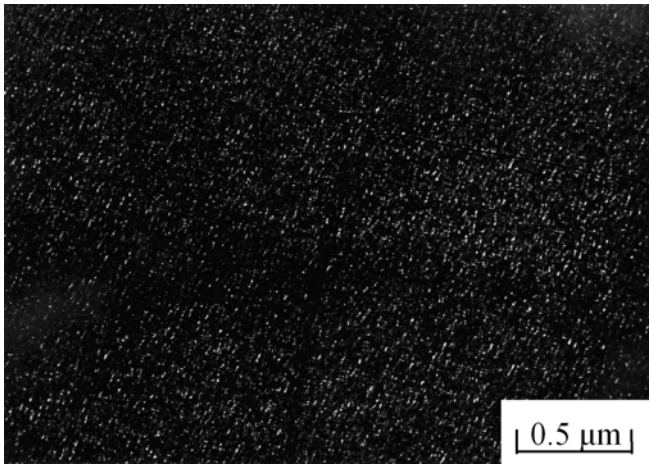

Figure 2.5(f)

Figure 2.5 Electron micrographs of the as-quenched $Cu_{2.6}Mn_{0.4}Al$ alloy. (a) BF, (b) and (c) two SADPs. The zone axes of the $D0_3$ phase are [100] and [110], respectively. (hkl= ($D0_3$ + $L2_1$) phase, hkl_{1or2}= L-J phase, 1: variant 1; 2: variant 2). (d) and (e) ($\bar{1}11$) and (002) $D0_3$ DF, respectively, (f) (100_1) L-J DF.

On the basis of the preceding results, it can be concluded that in the as-quenched condition, the L-J phase was present in the $Cu_{3-x}Mn_xAl$ alloys with X=0.2, 0.3 and 0.4, whose amount increased with increasing Mn content. Besides, the β → B2 → ($D0_3$ + $L2_1$) transition had occurred during quenching in the $Cu_{2.6}Mn_{0.4}Al$ alloy. These observations are consistent with those proposed by Bouchard et al. [1]. However, when the $Cu_{3-x}Mn_xAl$ alloys with X=0.1, 0.2 and 0.3 were solution treated followed by a rapid quench, the β → B2 → $D0_3$ transition instead of the β → B2 → ($D0_3$ + $L2_1$) transition was found to occur. This finding is different from the previous proposition in the $Cu_{3-x}Mn_xAl$ alloys with $0.1 \leqq X \leqq 0.8$ [1].

In Fe-Al and Fe-Al-Mn alloys, it is well-known that if the $D0_3$ phase was formed by continuous ordering transition during quenching, it would always occur through an A2 (disordered body-centered cubic) → B2 → $D0_3$ transition. The A2 → B2 transition produced the a/4<111> APBs and the B2 → $D0_3$ transition produced the a/2<100> APBs [19-21]. However, to date, no a/4<111> APBs could be investigated by other workers in the as-quenched $Cu_{3-x}Mn_xAl$ alloys [1-2, 8]. In the present study, it is obvious that no evidence of the a/4<111> APBs could be observed in the $Cu_{2.6}Mn_{0.4}Al$ alloy. However, when the Mn content was decreased to 7.5 at.% or below, the a/4<111> APBs became visible, as shown in Figures 2.3(f) and 2.4(d).This result implies that in the $Cu_{3-x}Mn_xAl$ alloys, an increase of the Mn content would increase the B2 domain size significantly. When the Mn content increased to above 10.3 at.%, the B2 domain size would consume to the whole grain during quenching. Therefore, no a/4<111> APBs could be detected. This may be one possible

reason to account for the absence of the a/4<111> APBs in the previous studies of the as-quenched $Cu_{3-x}Mn_xAl$ alloys with $0.5 \leqq X \leqq 1.0$ [1-2, 8].

Finally, it is worthwhile to note that the size of the $D0_3$ domains increased with increasing the Mn content. This implies that an increase of the Mn content would increase the B2 → $D0_3$ ordering transition temperature. This result is comparable to that obtained by Bouchard et al. [1].

2-4 Conclusions

The as-quenched microstructures of the $Cu_{3-x}Mn_xAl$ alloys have been studied by using optical microscopy and scanning transmission electron microscopy.

1. The as-quenched microstructure of the $Cu_{2.9}Mn_{0.1}Al$ alloy was of $D0_3$ phase containing plate-like γ_1' martensite, where the $D0_3$ phase was formed through the $\beta \rightarrow B2 \rightarrow D0_3$ transition during quenching. This is different from that reported by other workers in the Cu_3Al alloy.

2. The as-quenched microstructure of the $Cu_{2.8}Mn_{0.2}Al$ and $Cu_{2.7}Mn_{0.3}Al$ alloy was $D0_3$ phase containing extremely fine L-J precipitates, where the $D0_3$ phase was formed through the $\beta \rightarrow B2 \rightarrow D0_3$ transition during quenching.

3. The as-quenched microstructure of the $Cu_{2.6}Mn_{0.4}Al$ alloy was a mixture of ($D0_3$ + $L2_1$ + L-J) phases, where the ($D0_3$ + $L2_1$) phases were formed through the $\beta \rightarrow B2 \rightarrow (D0_3 + L2_1)$ transition during quenching.

4. The sizes of both B2 and $D0_3$ domains increased with increasing Mn content. This implies that an increase of the Mn content would increase A2 $\rightarrow$B2 and the $B2 \rightarrow D0_3$ ordering transition temperature. In addition, in the $Cu_{2.9}Mn_{0.1}Al$, $Cu_{2.8}Mn_{0.2}Al$ and $Cu_{2.7}Mn_{0.3}Al$ alloys, the a/4<111> APBs could be clearly observed. However, no evidence of the a/4<111> APBs

could be detected in the $Cu_{2.6}Mn_{0.4}Al$ alloy.

5. The amount of the L-J precipitates increased with increasing the Mn content.

References

1. M. Bouchard, G. Thomas: Acta Metall. 23 (1975) 1485.
2. Y. G. Nesterenko, I. A.Osipenko, S. A. Firstov: Fiz. Met. Metalloved. 27 (1969) 135.
3. Y. G. Nesterenko, I. A.Osipenko: Fiz. Met. Metalloved. 36 (1973) 702.
4. R. Kozubski, J. Soltys, J. Dutkiewicz, J. Morgiel: J. Mater. Sci. 22 (1987) 3843.
5. S. Sugimoto, S. Kondo, H. Nakamura, D. Book, Y. Wang, T. Kagotani, R. Kainuma, K. Ishida, M. Okada, M. Homma: J. Alloy. Compd. 265 (1998) 273.
6. R. Kainuma, N. Satoh, X.J. Liu, I. Ohnuma, K. Ishida: J. Alloy. Compd. 266 (1998) 191.
7. E. Obradó, C. Frontera, L. Mañosa, A. Planes: Phys. Rev. B 58 (1998) 14245.
8. S. C. Jeng, T. F. Liu: Metall. Mater. Trans. A 26A (1995) 1353.
9. C.L. Castillo, B.G. Mellor, M.L. Blázquez, C. Gómez: Scripta Metall. 21 (1987) 1711.
10. C.L. Castillo, M.L. Blázquez, C. Gómez, B.G. Mellor, N.Diego, J. Rio: J. Mater. Sci. 23 (1988) 3379.
11. M.L. Blazquéz, C.L. Castillo, C. Gómez: Metallography 23 (1989) 119.
12. T. F. Liu, J.S. Chou, C. C. Wu: Metall. Trans. A 21A (1991) 1891.
13. T. F. Liu, G. C. Uen, C. Y. Chao, Y. L. Lin, C. C. Wu: Metall. Trans. 22A (1991) 1407.

14. C. C. Wu, J. S. Chou, T. F. Liu: Metall. Trans. A. 22A (1991) 2265.

15. C. H. Chen, T. F. Liu: Metall. Mater. Trans .A 34A (2003) 503.

16. F. C. Lovey, V. G. Tendeloo, V. J. Landuyt, S. Amelinckx: Scripta Metall. 19 (1985) 1223.

17. N. Kuwano, C. M. Wayman: Metall. Trans. A 15A (1984) 621.

18. T. Hara, T. Ohba, S. Miyazaki, K. Otsuka: Mater. Trans. JIM 33 (1992) 1105.

19. P. R. Swann, W. R. Duff, R. M. Fisher: Metall. Trans. 3 (1972) 409.

20. S. M. Allen, J. W. Chan: Acta Metall. 24 (1976) 425.

21. J. W. Lee, T. F. Liu: Mater. Chem. Phys. 69 (2001) 192.